International Journal of Thermophysics, Vol. 17, No. 6, 1996

An Apparatus for Infrared Transmittance and Reflectance Measurements at Cryogenic Temperatures

Z. M. Zhang,[1,2] L. M. Hanssen,[3] R. U. Datla,[3] and H. D. Drew[4]

Received February 23, 1996

A facility for measuring the optical properties of solid materials at cryogenic temperatures is being developed at the National Institute of Standards and Technology. A cryostat that houses four bolometric detectors and a six-position sample holder was designed and built. The bolometers operate near 5 K, and the sample temperature can be varied from 6 to 100 K. The beam from a Fourier transform spectrometer is directed to the cryostat by reflective optical components. The measurable wavelengths extend from 1 μm to 1 mm, with appropriate sources and beamsplitters in the spectrometer as well as windows and detectors in the cryostat. The angle of incidence on the sample ranges from 7.5 to 60°. The mechanical, electrical, and optical designs are described in this paper. Initial measurement results at wavelengths from 2 to 30 μm and a sample temperature of 10 K are presented.

KEY WORDS: cryogenics; radiative properties; reflectance; transmittance.

1. INTRODUCTION

Studies of the infrared properties of materials at cryogenic temperatures are important to understanding the physical properties of novel materials [1–5], characterizing optical filters [6], and developing cryogenic radiometers [7, 8]. Measurements at cryogenic temperatures are difficult because of a combination of optical, electrical, mechanical, and thermal constraints. We have designed a unique cryogenic optical apparatus for measuring

[1] Department of Mechanical Engineering, University of Florida, Gainesville, Florida 32611, U.S.A.

[2] To whom correspondence should be addressed.

[3] Radiometric Physics Division, National Institute of Standards and Technology, Gaithersburg, Maryland 20899, U.S.A.

[4] Department of Physics, University of Maryland, College Park, Maryland 20742, U.S.A.

840/17/6-15

spectral transmittance and reflectance at wavelengths from 1 μm to 1 mm and for sample temperatures from 6 to 100 K. It is used together with a commercial rapid-scan Fourier transform spectrometer. This paper describes the cryogenic optical apparatus, the detector electronics, and the optical arrangements between the spectrometer and the cryostat. Initial test results are presented and methods to improve the measurement accuracy are discussed.

2. THE CRYOGENIC OPTICAL APPARATUS

The custom-designed cryostat, built by Infrared Laboratories, Inc.,[5] is shown in Fig. 1. It consists of a liquid-nitrogen container, a liquid-helium container, and a test chamber surrounded by radiation shields. The radiation shields are covered with aluminum foils except for the inner surface of the helium-temperature shield, which is black anodized to absorb the stray scattered radiation. The outside dimensions of the cryostat are approximately 60 cm in height and 30 cm in diameter. The volume of the liquid helium container is about 6 L. The hold time for liquid helium is $\approx$18 h. A six-position sample wheel, located at the center of the test chamber, can be tilted to vary the angle of incidence from 7.5 to 60° and rotated to change samples. Two wedged input windows are installed on the cryostat: a KRS-5 window for the wavelength range from 1 to 30 μm and a polyethylene window for the wavelength range from 30 μm to 1 mm. The wedging reduces interference effects, which is especially important for the far-infrared measurements. Four composite silicon bolometers are mounted in a 2×2 array assembly. Compound parabolic concentrators are used to collect incident radiation onto the bolometer absorbing elements. Each bolometer is designed for use in a specific wavelength range which is partially determined by a cold filter located at the front of its concentrator. The detector assembly can be rotated around the sample wheel to measure transmittance and directional reflectance. Four silicon diodes are used to monitor the temperature at different locations inside the cryostat. The temperature sensors are affixed to the detector mount, sample wheel stage, sample wheel, and one of the samples. They have been calibrated to within an uncertainty of 30 mK (expanded uncertainty with coverage factor of 2 is used in this paper). A heater and a temperature controller are used to control the temperature of the sample wheel to within $\pm$50 mK of a

[5] Trade names and company products mentioned in the text or identified in an illustration are used only to adequately specify the experimental procedure and equipment used. In no case does such identification imply recommendation or endorsement by the National Institute of Standards and Technology, nor does it imply that the products are necessarily the best available for the purpose.

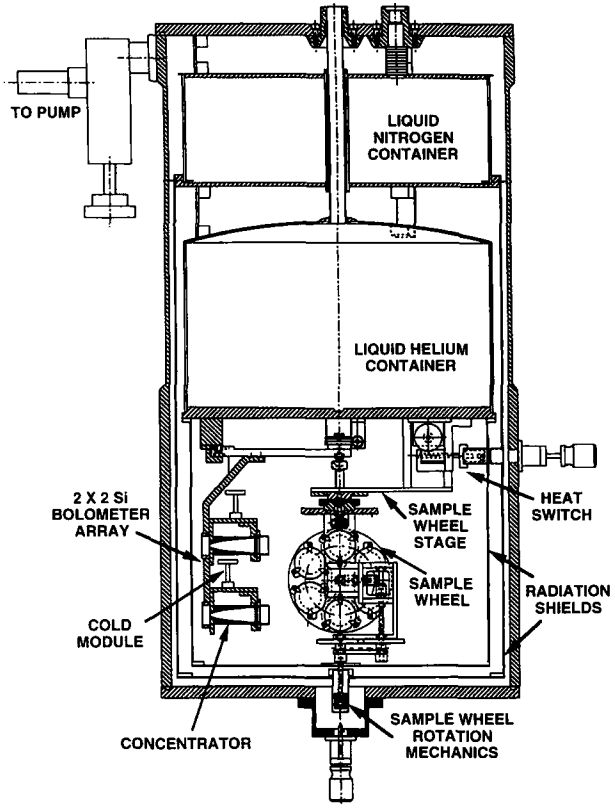

Fig. 1. Schematic diagram of the cryogenic optical apparatus.

Table I. Detector, Cold Filter, Window, Source, and Beamsplitter Configurations for Different Wavelength Regions

		Cryostat		Spectrometer	
Wavelength region (μm)	Detector No.	Cold filter	Window	Source	Beamsplitter
1–3	1	ZnSe	KRS-5	Tungsten halogen	Quartz
2–19				Globar	KBr
15–30	2	CdTe (w/ coating)	KRS-5	Globar	3-μm Mylar
30–100	3	Sapphire (w/ coating)	Polyethylene	Globar	6-μm Mylar
100–500	4	Quartz (w/ coating)	Polyethylene	Mercury arc	25-μm Mylar
300–1000					50-μm Mylar

selected temperature. A heat switch, shown in Fig. 1, is used to vary the contact thermal resistance between the sample wheel stage and the liquid-helium reservoir. Infrared radiation comes from a Bomem DA-3 Fourier transform spectrometer. The output spectral range is determined by the source and beamsplitter of the spectrometer. Table I lists the configurations for different wavelength regions. The novelty of this apparatus lies in the integration of sample holder and detectors in a single cryostat, the capability of both transmittance and directional reflectance measurements, and the wide wavelength and temperature ranges.

3. THE SILICON BOLOMETERS

A bolometer measures radiant power by detecting the induced temperature change. It is based on the temperature dependence of electrical resistance of certain materials, such as semiconductors and superconductors [9, 10]. In this work, four custom-designed silicon bolometers are employed. The resistive elements are made of doped-silicon crystals (approximate dimensions: $0.4 \times 0.4 \times 0.3$ mm). The Si crystal is attached to a diamond disk (2.5 mm in diameter and 100 μm thick). A Bi coating is deposited on the back of the diamond substrate for each bolometer to increase its absorptance [11]. Gold-coated concentrators are used to focus the radiation onto the detector elements. The electrical leads are made of copper wires, which also serve as thermal links between the detector element and the heat sink (i.e., the detector mount). The four bolometers are essentially the same, except that the diameter of the Cu leads is 125 μm for detector 1 and 75 μm for the others. Therefore, the thermal conductance between the sensing element and the heat sink for detector No. 1 is greater than that for the others. This improves its speed at the price of a reduced responsivity. A fast response is required for detector 1 since it is used for the shortest wavelength region ($1 < \lambda < 19$ μm), which corresponds to the highest-modulation-frequency region for a fast-scan Fourier transform spectrometer.

The electronic diagram of a bolometer is shown in Fig. 2. The bolometer and the load resistor are near the liquid-helium temperature. The ac preamplifier operates at room temperature. The junction field effect transistors (JFET) are mounted on the cold modules inside the cryostat (see Fig. 1). The cold modules were maintained near 70 K using electrical heating (power dissipation, <1 mW). The input impedance of the JFET is greater than $10^{13}\Omega$. The bolometer equations are [12, 13]

$$I_{\text{bias}} = V_{\text{bias}}/(R_{\text{L}} + R_{\text{B}}) \tag{1}$$

$$V_{\text{s}} = I_{\text{bias}} R_{\text{B}} \tag{2}$$

For $\Delta R_B \ll (R_L + R_B)$, the signal voltage is

$$\Delta V_s = \frac{\Delta R_B R_L V_{bias}}{(R_L + R_B)^2} \tag{3}$$

which is proportional to the resistance change of the bolometer. The resistance change is related to the temperature change. Using a simple thermal model described by Putley [9], it can be shown that the change of amplitude of temperature is

$$\Delta T = \frac{\alpha \Delta P}{G(1 + \omega^2 \tau^2)^{1/2}} \tag{4}$$

where α is the absorptance, ΔP is the amplitude of the radiant power reaching the detector, ω is the modulation frequency, G is the effective thermal conductance, and τ is the thermal time constant. The responsivity, $S = \Delta V_s / \Delta P$, of a bolometer is

$$S = \frac{\alpha}{G(1 + \omega^2 \tau^2)^{1/2}} \frac{R_L V_{bias}}{(R_L + R_B)^2} \frac{dR_B}{dT} \tag{5}$$

R_B and dR_B/dT are functions of the operating temperature of the bolometer, which is higher than the temperature of the heat sink due to the bias current, background radiation, and the incident radiation. The time constant of the silicon bolometers used in this work is a few milliseconds.

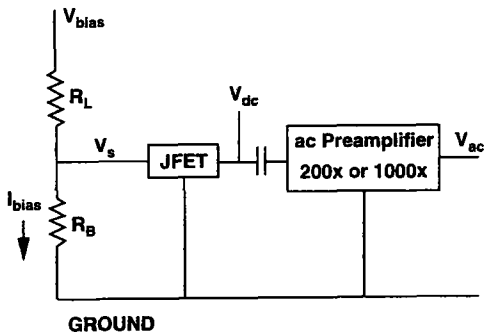

Fig. 2. Electronic scheme of a bolometer. JFET—junction field effect transistor; I_{bias}—bias current; R_B—bolometer resistance; R_L—load resistor; V_{bias}—bias voltage; V_{ac}—ac output voltage; V_{dc}—dc output voltage; V_s—bolometer voltage.

When the heat sink temperature is near 5 K, the bolometer responsivity for electrical power, estimated from the load curve [14], is $\approx 10^5$ V · W^{-1} with $I_{\text{bias}} \approx 2$ μA. The noise equivalent power of the bolometers (NEP) is measured to be $\approx 10^{-12}$ W · Hz$^{-1/2}$ at 80 Hz using a spectrum analyzer. As the temperature increases, the responsivity decreases and the NEP increases. At a temperature of 6 K, the responsivity decreases by almost an order of magnitude. The responsivity is also a function of the modulation frequency. The infrared beam from the Fourier transform spectrometer is modulated at a modulation frequency proportional to the optical frequency and the speed of the moving mirror [15]. Hence, the responsivity decreases rapidly as the wavelength is decreased below a characteristic value corresponding to the roll-off frequency of the bolometer. The speed of the moving mirror was chosen to be 0.5 cm · s^{-1} for $2 < \lambda < 30$ μm. This corresponds to a modulation frequency of 2 kHz at $\lambda = 5$ μm and 400 Hz at $\lambda = 25$ μm.

4. THE OPTICAL DESIGN

The beam coming out of the spectrometer is collimated and its diameter is 75 mm. The clear aperture of the cryostat window and the cold filters is ≈ 12 mm in diameter. Three gold-coated mirrors are used to condition the beam, as shown in Fig. 3. A ray-tracing program was used to facilitate the design. After a plane mirror, a 90° off-axis paraboloidal mirror (focal length = 75 mm) focuses the beam to one of the focal points of an ellipsoidal mirror. The sample position is at the other focal point of the ellipsoidal mirror (the distance between the two focuses of the ellipsoid is

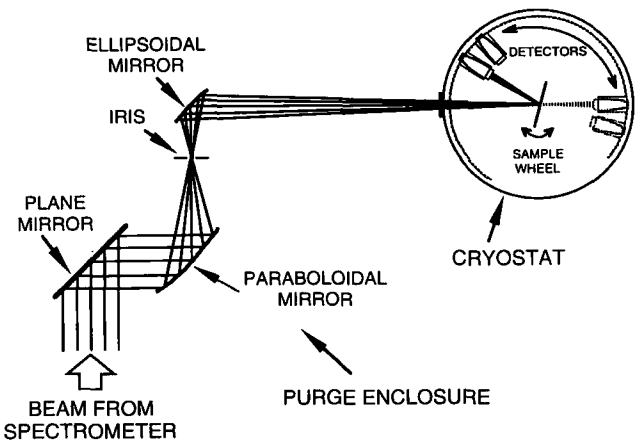

Fig. 3. Schematic diagram of the optical arrangements.

508 mm). The ellipsoidal mirror is designed such that the reflected beam is perpendicular to the incident beam at the optical axis.

A 4-mm-diameter iris was placed at the common focus of the paraboloidal and ellipsoidal mirrors to facilitate the alignment and to eliminate inter-reflection between the spectrometer and the cryostat window. The spectrometer is equipped with a visible source and beamsplitter, which was used for alignment of the mirrors and cryostat. The beam spot size on the sample is determined by the source aperture of the spectrometer. By energy conservation, the throughput, which is the product of the projected surface area and the solid angle, of a beam cannot be increased. The clear aperture diameter of the window is $d \approx 12.5$ mm, and the distance between the sample and the window is $L \approx 150$ mm. The f-number is $L/d \approx 12$. Since the f-number at the source aperture of the spectrometer is 4, the diameter of the beam spot at the sample should be approximately three times that of the aperture. Due to the imperfections of the optical components and alignment, the actual beam spot is about twice as large as the theoretical value. The beam spot diameter is ≈ 6 mm at the sample location and ≈ 11 mm at the window location with a source aperture of 1 mm in diameter. A He–Ne laser was used to test the alignment inside the cryostat and the beam deviation due to the wedged KRS-5 window.

A Plexiglas enclosure was made to cover the coupling optics. CO_2-free dry air was used to purge the spectrometer and the enclosure. The spectrometer is sealed with O-rings and can be evacuated down to 100 Pa. For measurements at $\lambda > 100$ μm, it may be necessary to build an enclosure that can be evacuated to reduce the residual water vapor absorption.

5. MEASUREMENT RESULTS AND DISCUSSION

We have tested the cryostat performance by using various samples, including an interference filter, a silicon wafer, and a copper disk with an aperture.

The detector mount temperature was 5.67 K for transmittance measurements and 5.97 K for reflectance measurements. The detector temperature varies as the bolometer assembly is moved to different positions in the cryostat. This may be caused by differences in the thermal contact or radiation background. The temperature of the sample wheel stage was near 6 K, and the temperatures of the sample and sample wheel remained stable near 10 K without using the temperature controller.

One of the six positions on the sample wheel was left blank for the transmittance reference measurements. A gold mirror was used as the reflectance reference sample. It was made by vacuum depositing a gold film (200 nm thick) on a silicon substrate. The reflectance of gold film is greater than 0.99 at low temperatures for $\lambda > 2$ μm [16]. The mirror reflectance is

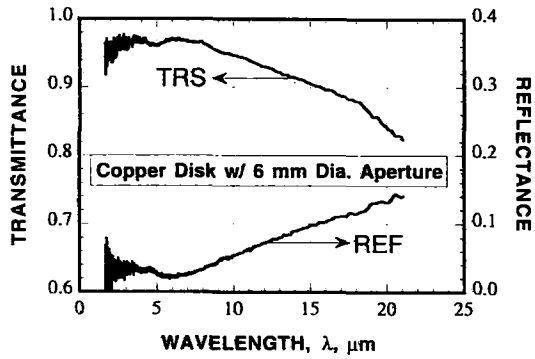

Fig. 4. Measured transmittance and reflectance of a copper disk with a 6-mm-diameter aperture.

taken to be 1. Repeated measurements indicated that the system stability is at the 1% level. The mechanical repeatability of the sample positions is almost perfect. The zero-level transmittance was obtained by blocking the beam with the mirror, and the zero-level reflectance was obtained with the blank in the sample position. The zero level is <0.0002 in transmittance and <0.001 in reflectance. At $\lambda > 5$ μm, the peak-to-peak noise level is <0.002 in transmittance and <0.005 in reflectance. The above measurements were made with a 1-mm-diameter source aperture and coadded for 400 scans.

One of the samples is made of a polished copper disk with a 6-mm-diameter aperture, which is used to examine the beam spot size at the sample wheel. The radiation comes from both the source and the aperture wall, which emits and reflects room-temperature radiation. The transmittance and reflectance spectra of the disk are shown in Fig. 4. At $\lambda < 5$ μm, the transmittance is ≈ 0.97 and the reflectance is ≈ 0.03, indicating that the effective beam spot diameter is close to 6 mm. The transmittance goes down and reflectance goes up with increasing wavelength, indicating that the beam spot size increases with wavelength. Radiation from the wall of the source aperture, which is near 300 K, may have influenced the effective beam spot size at longer wavelengths. The Globar source used in the spectrometer operates near 1200 K. The power emitted from a blackbody at temperature T is given by the Planck distribution function [17]

$$e_b(\lambda, T) = \frac{2\pi hc^2}{\lambda^5[\exp(hc/kT\lambda) - 1]} \tag{6}$$

where $h = 6.626 \times 10^{-34}$ J · s is Planck's constant, $k = 1.38 \times 10^{-23}$ J · K^{-1} is the Boltzmann constant, and $c = 3 \times 10^8$ m · s^{-1} is the speed of light in

vacuum. The ratio of two blackbodies at temperatures of T_a (room temperature) and T_s (source temperature) is

$$\frac{e_b(\lambda, T_a)}{e_b(\lambda, T_s)} = \frac{\exp(hc/kT_s\lambda) - 1}{\exp(hc/kT_a\lambda) - 1} \tag{7}$$

The above equation approaches 0 as $\lambda \to 0$, and T_a/T_s as $\lambda \to \infty$. For $T_a = 300$ K and $T_s = 1200$ K, the ratio is less than 0.001 for $\lambda < 5$ μm, 0.02 at $\lambda = 10$ μm, and 0.08 at $\lambda = 20$ μm. Since the effective area of the wall of the aperture is much greater than that of its opening, the amount of radiation from the wall of the aperture is large enough to effectively increase the beam spot size on the sample. The emissivity of the Globar source is greater than 0.80 [18]. The wall of the aperture emits and reflects room-temperature radiation. With a DTGS detector, we have blocked the source aperture using materials of different emissivity. The resulting spectra are almost-identical. The ratio of the spectrum with the aperture blocked to that with the aperture open increases at long wavelengths.

A second aperture may be used after the spectrometer (in place of the iris in Fig. 3) to limit the beam spot size on the sample. The radiation from the wall of the aperture outside the spectrometer is not modulated and, therefore, will not contribute to the interferogram. However, the alignment will be more difficult to achieve. This method needs to be investigated further. In the following measurements of a Si wafer and an interference filter, the clear aperture diameter of the sample holder is 18 mm. Therefore, the infrared beam always underfills the samples.

The transmittance and reflectance of a crystalline silicon wafer (0.5 mm thick and 25 mm in diameter) measured under different conditions are shown in Fig. 5. The Si sample is boron doped at a concentration of $1.3\text{–}2.2 \times 10^{14}$ atoms $\cdot$ cm^{-3}, and its electrical resistivity is greater than 60 $\Omega \cdot$ cm at room temperature. The silicon wafer is used to check the radiometric accuracy of the measurements since the refractive index of silicon does not change appreciably with temperature [1, 19]. The room-temperature transmittance of this Si wafer, measured with a DTGS detector, is shown in Fig. 5a for comparison. A resolution of 8 cm^{-1} was used, which is greater than the free spectral range, $\Delta(1/\lambda) = (2nt)^{-1} \approx 3$ cm^{-1}, where n is the refractive index and t is the thickness of the Si sample. Hence, the transmittance and reflectance can be predicted using geometric optics considering multiple internal reflections [20]. In the region where absorption can be neglected, the transmittance is

$$\text{TRS} = \frac{2n}{n^2 + 1} \tag{8}$$

and the reflectance is REF = 1 − TRS. The room-temperature transmittance of the Si wafer (see Fig. 5) at wavelengths between 2 and 6 μm agrees with that calculated from the reported refractive index of silicon within 1% [21].

At 10 K, with a source aperture diameter of 1 mm, the measured transmittance is $\approx$0.60 and the reflectance is $\approx$0.48 for wavelengths less than 6 μm. The sum of the transmittance and reflectance is greater than 1, indicating a systematic error in the measurements. The radiometric accuracy of Fourier transform spectrometry can be affected by detector nonlinearity and responsivity change. The most prominent signature of nonlinearity is in the region beyond the long wavelength cutoff, since detector nonlinearity causes a nonzero response, i.e., nonphysical signal [22]. This did not occur in the response spectra for both the sample and the reference. The other mechanism is due to the change in the detector responsivity between the

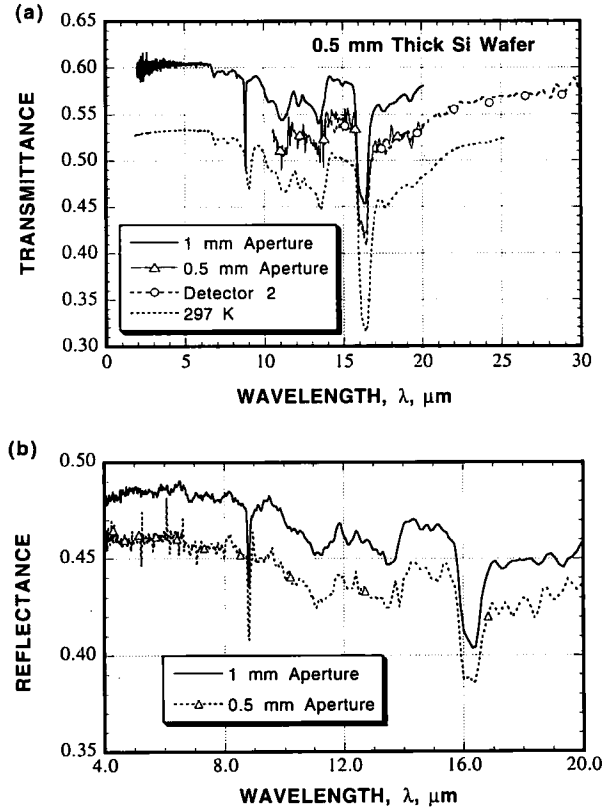

Fig. 5. Measured transmittance and reflectance of a silicon wafer.

sample run and the reference run, which was called nonequivalent detector responsivity by Flik and Zhang [23]. The responsivity of a bolometer is given in Eq. (5), where R_B and dR_B/dT depend on the operating temperature. In general, the responsivity increases as temperature decreases. Since the average power reaching the detector for the sample run is less than that for the reference run, the responsivity for the sample run is greater than that for the reference run. This could result in a measured TRS or REF greater than the actual values. By reducing the power level either using a neutral-density filter (transmittance ≈ 0.10 in the spectral region of interest) or using a smaller-diameter source aperture, the measured TRS and REF decreased as shown in Fig. 5. The reduction is almost a constant factor independent of wavelength. This is consistent with the mechanism of non-equivalent detector responsivity [23]. The measured transmittance for $15 < \lambda < 30$ μm with detector 2 (using a 2.5-mm-diameter source aperture) overlapped that measured with detector 1 using a 0.5-mm-diameter source aperture. The change in responsivity is smaller in this case with detector 2 because the cold filter blocked the radiation at $\lambda < 15$ μm. The disadvantage of reducing the optical power is the decreased signal-to-noise ratio as seen in Fig. 5. Another method to reduce the effect of nonequivalent detector responsivity is to increase the bias current. However, the electrical power applied to the bolometer is only a few microwatts, while the power of the incident radiation that reaches the bolometer can be several tenths of a milliwatt. Therefore, the change of responsivity cannot be compensated by increasing the bias current.

As shown in Fig. 2, both V_{dc} and V_{ac} can be measured. The operating point (R_B) of the detector is

$$R_B = \frac{V_{dc} R_L}{V_{bias} - V_{dc}} \tag{9}$$

In a different run, the detector mount temperature was 5.74 K. For bolometer 1 with a source aperture of 1-mm diameter, it was found that $R_B \approx 529$ kΩ with an interference filter, $R_B \approx 487$ kΩ with the Si wafer, and $R_B \approx 450$ kΩ with the blank. In the reflectance measurements, the detector mount temperature was 6.05 K, and $R_B \approx 333$ kΩ with the Si wafer and $R_B \approx 303$ kΩ with the Au mirror. This indicates that indeed there is a large change in the operating point of the bolometer due to the incident radiation. In the future, the detector responsivity will be characterized and corrections will be made to account for the change of responsivity. In a recent review, Richards [24] discussed methods for characterizing low-temperature bolometers and compensating for the responsivity change.

With a 0.5-mm-diameter source aperture, the uncertainty level is estimated to be 5% including the uncertainty due to the responsivity change.

Absorption due to lattice vibration and interstitial oxygen in the wavelength region from 6 to 25 μm can be seen in Fig. 5. The absorption band of interstitial oxygen at 9.0 μm [25] becomes stronger and narrower at low temperatures and is shifted to a shorter wavelength at 8.8 μm. The fine absorption structure of oxygen absorption bands in Si at low temperatures was discussed by Ryoo et al. [26].

The effect of temperature and angle of incidence on an interference filter was investigated. The transmittance spectra normalized to the maximum transmittance are shown in Fig. 6. The normalized transmittance of this sample at room temperature, measured by Zhang et al. [27], is also shown. The transmittance band is near 4 μm with a FWHM (full width at half-maximum) of 0.2 μm. The transmission band shifts significantly toward short wavelengths from room temperature to 10 K ($\approx$0.08 μm). The transmission band also shifts with the angle of incidence. At 10 K, it shifts about -0.02 μm from 0 to 15° and about -0.05 μm from 15 to 30°. As discussed by Stierwalt [6], the wavelength of the transmission band can shift in either direction due to changes of temperature. The measured result reinforces the importance of characterizing filters at the same temperature and angle of incidence as they are used in practice. The maximum transmittance at room temperature is measured to be $\approx$0.9. The measured maximum transmittance at 10 K is greater than 1, which is also attributed to a change of the detector responsivity caused by different incident radiation power.

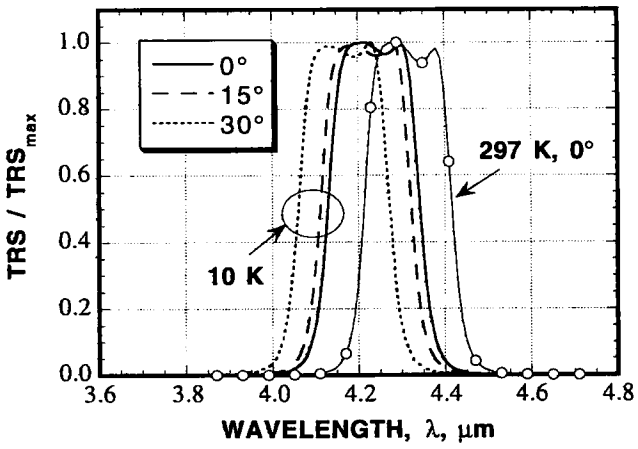

Fig. 6. Normalized transmittance of an interference filter.

6. CONCLUSIONS AND FUTURE RESEARCH

A cryogenic optical apparatus was designed, built, and tested with a Fourier transform spectrometer. Reflective optical components were used to interface the spectrometer with the cryostat. Transmittance and reflectance measurements were made for several samples at 10 K and at wavelengths from 2 to 30 μm. Measurements of a copper disk with a 6-mm aperture demonstrated proper alignment. The beam spot diameter at the sample was near 6 mm for $\lambda < 5$ μm with a source aperture of 1 mm. Radiation from the standard aperture can increase the beam spot size for $\lambda > 5$ μm. Results from the measured transmittance and reflectance of a silicon wafer suggested that the responsivity of the detector was not the same for the sample run as that for the reference run. This could cause an error of a few percent in the measurements. Reducing the optical power improves the radiometric accuracy but deteriorates the signal-to-noise ratio. A wavelength shift of the transmission band has been observed for a bandpass filter with a bandpass near 4 μm.

In the future, the response curves of the bolometers will be measured and correction methods will be implemented to account for the change of the detector responsivity with input power. A second aperture between the paraboloidal mirror and the ellipsoidal mirror will be used as the limiting aperture to reduce the beam spot size on the sample. A vacuum enclosure will be designed for longer wavelengths. Methods to reduce the sample temperature and detector mount temperature will be investigated. This facility will be applied to measure accurately the radiative properties of various materials, including infrared filters, black coatings, and high-temperature superconducting films.

ACKNOWLEDGMENTS

This work has been funded by the BMDO, Newark AFB, Ohio. The authors would like to thank G. P. Eppeldauer of the National Institute of Standards and Technology and C. G. Malone of the Massachusetts Institute of Technology for helpful discussions. Z.M.Z. acknowledges the support of the National Institute of Standards and Technology through a Guest Scientist appointment.

REFERENCES

1. E. V. Loewenstein, D. R. Smith, and R. L. Morgan, *Appl. Opt.* **12**:398 (1973).
2. M. I. Flik, Z. M. Zhang, K. E. Goodson, M. P. Siegal, and J. M. Phillips, *Phys. Rev. B* **46**:5606 (1992).

3. K. Karrai, E. J. Choi, F. Dunmore, S. Liu, H. D. Drew, Q. Li, D. B. Fenner, Y. D. Zhu, and F. C. Zhang, *Phys. Rev. Lett.* **69**:152 (1992).
4. Z. M. Zhang, B. I. Choi, M. I. Flik, and A. C. Anderson, *J. Opt. Soc. Am. B* **11**:2252 (1994).
5. Y. Okimoto, T. Katsufuji, T. Ishikawa, A. Urushibara, T. Arima, and Y. Tokura, *Phys. Rev. Lett.* **75**:109 (1995).
6. D. L. Stierwalt, in *Infrared Thin Films*, R. P. Shimshock, ed. (SPIE Critical Reviews, Vol. 39, Bellingham, WA, 1991), pp. 181–195.
7. R. U. Datla, K. Stock, A. C. Parr, C. C. Hoyt, P. J. Miller, and P. V. Foukal, *Appl. Opt.* **31**:7219 (1992).
8. Z. M. Zhang, R. U. Datla, S. R. Lorentz, and H. C. Tang, *J. Heat Transfer* **116**:993 (1994).
9. E. H. Putley, in *Optical and Infrared Detectors*, 2nd ed., R. J. Keyes, ed. (Springer-Verlag, Berlin, 1980), Chap. 3.
10. Z. M. Zhang and A. Frenkel, *J. Superconduct.* **7**:871 (1994).
11. J. Clarke, G. I. Hoffer, P. L. Richards, and N. H. Yeh, *J. Appl. Phys.* **48**:4865 (1977).
12. G. Eppeldauer, A. L. Migdall, and C. L. Cromer, *Metrologia* **30**:317 (1993).
13. J. P. Makai, R. D. Saunders, and G. Dezsi, in *Infrared Technology XX*, B. F. Andresen, ed. (SPIE, Vol. 2269, Bellingham, WA, 1994), pp. 772–779.
14. F. J. Low, *J. Opt. Soc. Am.* **51**:1300 (1961).
15. P. R. Griffiths and J. A. de Haseth, *Fourier Transform Infrared Spectrometry* (John Wiley and Sons, New York, 1986), Chap. 1.
16. W. M. Toscano and E. G. Cravalho, *J. Heat Transfer* **98**:438 (1976).
17. R. Siegel and J. R. Howell, *Thermal Radiation Heat Transfer*, 3nd ed. (Hemisphere, Washington, DC, 1992), Chap. 2.
18. L. Genzel, in *Far-Infrared Properties of Solids*, S. S. Mitra and S. Nudelman, eds. (Plenum Press, New York, 1970), pp. 51–102.
19. H. W. Icenogle, B. C. Platt, and W. L. Wolfe, *Appl. Opt.* **15**:2348 (1976).
20. Z. M. Zhang, in *Heat Transfer* 1994—*Proceedings of the Tenth International Heat Transfer Conference*, G. F. Hewitt, ed. (Institution of Chemical Engineers, Rugby, UK, 1994), Vol. 2, pp. 177–182.
21. D. F. Edwards, in *Handbook of Optical Constants of Solids*, E. D. Palik, ed. (Academic Press, Orlando, FL, 1985), pp. 545–469.
22. D. B. Chase, *Appl. Spectrosc.* **38**:491 (1984).
23. M. I. Flik and Z. M. Zhang, *J. Quant. Spectrosc. Radiat. Transfer* **47**:293 (1992).
24. P. L. Richards, *J. Appl. Phys.* **76**:1 (1994).
25. B. G. Rennex, *NIST Special Publication 260-121* (U.S. Government Printing Office, Washington, DC, 1994).
26. K. Ryoo, H. R. Kim, J. S. Koh, G. Seo, and J. H. Lee, *J. Appl. Phys.* **72**:5393 (1992).
27. Z. M. Zhang, L. M. Hanssen, and R. U. Datla, *Opt. Lett.* **20**:1077 (1995).